Type of the Paper (Article)

Influence of the fibre distribution and orientation in the fracture behaviour of polyolefin fibre reinforced concrete

A. Enfedaque[1], M. G. Alberti[2], J.C. Gálvez[3,*]

[1] *Departamento de Ingeniería Civil: Construcción, E.T.S de Ingenieros de Caminos, Canales y Puertos, Universidad Politécnica de Madrid. C / Profesor Aranguren, s/n, 28040, Madrid.*; alejandro.enfedaque@upm.es

[2] *Departamento de Ingeniería Civil: Construcción, E.T.S de Ingenieros de Caminos, Canales y Puertos, Universidad Politécnica de Madrid. C / Profesor Aranguren, s/n, 28040, Madrid.*; marcos.garcia@upm.es

[3] *Departamento de Ingeniería Civil: Construcción, E.T.S de Ingenieros de Caminos, Canales y Puertos, Universidad Politécnica de Madrid. C / Profesor Aranguren, s/n, 28040, Madrid.*; jaime.galve@upm.es

* Correspondence: jaime.galve@upm.es; Tel.: +34-910674125

Abstract: Polyolefin fibre reinforced concrete (PFRC) has become an attractive alternative to steel for the reinforcement of concrete elements mainly due to its chemical stability and the residual strengths that can be reached with lower weights. The use of polyolefin fibres can meet the requirements in the standards, although the main constitutive relations are based on the experience with steel fibres. Therefore, the structural contributions of the fibres should be assessed by inverse analysis. In this study, the fibre dosage has been fixed at 6kg/m³ and both self-compacting concrete and conventional concrete have been used to compare the influence of the positioning of the fibres. An idealized homogeneous distribution of the fibres with such fibres crossing from side to side of the specimen has been added to self-compacting concrete. The experimental results of three-point bending tests on notched specimens have been reproduced by using the cohesive crack approach. Hence, the constitutive relations were found. The significance of this research relies on the verification of the formulations found to build the constitutive relations. Moreover, with these results it is possible to establish the higher threshold of the performance of PFRC and the difficulties of limiting the first unloading branch typical of fracture tests of PFRC.

Keywords: fibre reinforced concrete; polyolefin fibres; fibre distribution; fracture behaviour; structural fibres

---

1. Introduction

Reinforced concrete was the most relevant construction material employed both in architecture and civil engineering during the XX century. The widespread use of such material was widened in the second half of the century when fibres began to be added to common concrete formulations. Since that moment, the applications of fibre-reinforced concrete (FRC) have been drastically enlarged due to the development of a significant variety of fibres produced by combining materials, sizes and shapes [1-4]. The improvement of the concrete properties that the fibres induce has enabled a large amount of uses such as cracking control, fire spalling prevention, and multifunctional concretes [5-7] that enable applications such as guiding vehicles or heating pavements. In some of these uses, the metallic nature of steel fibres, which are the most common, might be an issue due to their potential corrodible and magnetic nature. In order to address such situations, certain types of polymeric fibres, which can be considered as structural ones, have recently been developed. Those fibres, essentially polyolefin-based macro fibres, provide structural capacities with lower dosages in terms of weight. In addition, polyolefin fibres (PF) are chemically stable and reduce the overall cost of the material.

Preprints (www.preprints.org) | NOT PEER-REVIEWED | Posted: 5 December 2018 doi:10.20944/preprints201812.0065.v1

Peer-reviewed version available at Materials 2019, 12, 220; doi:10.3390/ma12020220

Polyolefin fibre reinforced concrete (PFRC) has been the centre of relevant research in recent years, especially focussed on the characterization of the mechanical properties [8-13] and engineering applications [14, 15].

Fibres are added in the final stages of FRC production. Pouring methods, formwork geometry and rheological properties of concrete add variations in the positioning and orientation of the fibres, as examined in references [16, 17, 18]. Such parameters have been studied through employing a wide variety of means, for example, use of stereological tools [19], statistical ones [20] and even rheological analysis [21, 22]. Most of the studies that deal with this matter have counted the amount of fibres placed in a sawn surface or in the fracture surfaces generated in bending fracture tests [23, 24, 25]. In such cases, the orientation factor proposed by Krenchel in 1975 [26] enables the use of a parameter that offers a coupled value of the orientation and the distribution of the fibres. With the use of the orientation factor θ, it has been possible to determine the improvements in mechanical properties of SFRC by using self-compacting concrete (SCC) [27] and the effects of several types of vibration on conventional concrete (VCC) [23]. Nevertheless, at the time of writing there is a gap in experimental data and analytical models for predicting the upper threshold of the improvement that a certain amount of polyolefin fibres, if ideally oriented and distributed, can provide to a certain type of concrete.

The main improvement that fibres provide to concrete appears after concrete cracking has taken place. Consequently, such post-cracking behaviour has become the reference property, with several tests and recommendations being established [28-34] in order to enable a trustworthy comparison among the possible combinations of concrete and fibres. If the results comply with certain requirements established in the aforementioned recommendations, the contribution of the fibres added to the composite material might be taken into account, Therefore, it would be possible to reduce the amount of traditional steel rebars in reinforced concrete. Although this procedure is currently used, the development of predictive models that may allow the prediction of the number and positioning of the fibres placed in the critical sections of a structural piece is welcomed [35, 36, 27, 37, 38, 39]. Such models might be a valuable tool for structural designers; they would also entail merging the laboratory test results and the everyday structural calculations.

Following this rationale, it would be even more significant to reproduce the fracture behaviour of FRC, and especially PFRC due to the novelty of the material, by means of numerical simulations. This study adopts the cohesive crack approach. Since the fracture behaviour of PFRC shows hardening tri-linear curves have been used. Such a type of curves has been used for SFRC in cases of intermediate branches with soft-unloading or even flat stages [40, 41]. However, the need for a branch with recharging strength has recently entailed an accurate reproduction of the mechanical behaviour of PFRC [42, 43]. Such a contribution was able to predict the mechanical response of a PFRC with a determined amount of fibres by changing the parameters that define a tri-linear softening function. The variations of such parameters were performed based on several assumptions and performing an inverse analysis. By combining the parameters obtained in the iterative analysis with a numerical regression, the functions that define the parameters of the softening functions were defined. However, such assumptions and the functions that were deduced have not been corroborated yet.

In order to address such shortcomings in the field of PFRC, an experimental study has been performed with self-compacting concrete and conventional vibrated concrete with a fibre dosage of 6kg/m^3 of 60mm-long polyolefin fibres randomly distributed and named SCC6-60 and VCC6-60 respectively. Additionally, self-compacting concrete (SCC) with the same amount of fibres ideally positioned with a homogeneous distribution in the cross section of the concrete elements was manufactured and termed SCC6-430. The reinforcement capacity of the fibres added has been assessed by comparing the behaviour of the material when subjected to three-point bending fracture tests for the three compositions manufactured. In addition, the influence of the orientation factor has been determined by counting the fibres placed in the fracture surfaces generated. Moreover, the test results, including those obtained in the specimens with an ideal homogeneous distribution of fibres, have been reproduced by using the constitutive fracture model shown in [42]. The changes added to the parameters that define the softening function have been compared for the formulations and the

Preprints (www.preprints.org) | NOT PEER-REVIEWED | Posted: 5 December 2018 doi:10.20944/preprints201812.0065.v1

Peer-reviewed version available at Materials 2019, 12, 220; doi:10.3390/ma12020220

assumptions performed and the functions that define such variations analysed. The significance of this research lies in the definition of the threshold of the mechanical reinforcement of PFRC when the fibres are ideally distributed. In addition, the importance of the distribution of the fibres would be found when comparing the post-peak behaviour of SCC6-60 and the SCC6-60 with the behaviour of SCC6-430. Moreover, the assumptions made in references [8, 17] that established a relation between the maximum post-peak load (L_{REM}) and the number of fibres in the fracture surface generated are validated. In addition, the relation between the minimum post-cracking load and the amount of fibres in the lower third of the fracture surface generate is also validated. Besides, the numerical simulations performed would validate the hypothesis assumed in the literature and enable a confident use of the functions proposed. Thus, the accuracy of the numerical simulations and the inverse analysis can improve future modelling procedures and supply reliable constitutive relations for PFRC related with physical parameters.

2. Concrete production

Both vibrated concrete (VC) and SCC were manufactured with siliceous aggregates composed of two types of gravel of 4-8 mm and 4-12 mm and sand of 0-2 mm. The maximum aggregate size was 12.7 mm. A Portland cement type EN 197-1 CEM I 52.5 R-SR 5 [44] was used in this study. A mineral admixture of limestone powder as micro-aggregate was employed with specific gravity and Blaine surface of 2700 kg/m³ and 400-450 m²/kg, respectively. The calcium carbonate content of the limestone powder was higher than 98%, with less than 0.05% being retained in the 45 μm sieve. In the SCC and in the VC alike, an admixture named Sika Viscocrete 5720 (a polycarboxylate-based superplasticizer with a solid content of 36% and 1090 kg/m³ density) was employed. The formulations of VC and SCC can be seen in Table 1.

Table 1. Concrete formulation per m³.

	Cement	Limestone powder	Water	Sand	Gravel	Grit	Superplasticizer (% cement weight)
SCC6-60 and SCC6-430	375	200	187.5	918	245	367	1.25
VCC	375	100	187.5	916	300	450	0.75

In this study, the polyolefin fibres employed boasted two different lengths. Firstly, 60mm-long commercial fibres; and secondly, the same fibres but 600mm-long. Both fibres had the same mechanical and chemical properties and only differed in their length. The outlook of the 60mm long fibres where their rough surfaces appear can be seen in Figure 1. Likewise, the mechanical properties supplied by the manufacturer can be seen is such an illustration.

Density (g/cm³)	0.910
Length (mm)	60
Eq. diameter. (mm)	0.903
Tensile strength (MPa)	> 500
Modulus of elasticity (GPa)	> 9

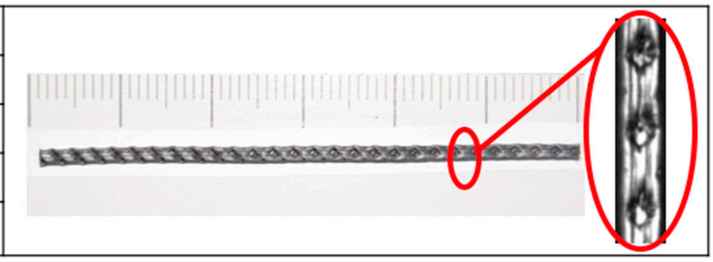

Figure 1. Commercial polyolefin fibre. Scale in mm. Mechanical properties supplied by the manufacturer.

With the aforementioned materials, three types of concrete were prepared. The first two were a vibrated conventional concrete and the second one a self-compacting concrete. In these two concretes, 6kg/m³ of the 60mm-long polyolefin commercial fibres previously described were used. In addition

doi:10.20944/preprints201812.0065.v1

Peer-reviewed version available at Materials 2019, 12, 220; doi:10.3390/ma12020220

to VCC6-60 and SCC6-60, other specimens were manufactured with the same volumetric fraction of fibres but choosing the position and orientation of the fibres. This batch was named SCC6-430. In SCC6-60 a standard mixing procedure was used. The fibres were added in three stages and consequently were mixed with the rest of components, leading to a random positioning of the fibres within the bulk. Once the VCC6 concrete was prepared, the material was poured in 430x100x100mm^3 moulds following the recommendation [30, 32]. In the case of the SCC6-60, the fresh material was poured from one of the sides of the mould to allow the fibres to align in the direction of the flow.

In the case of the SCC6-430, the fibres were positioned by choosing a homogeneous distribution and a perpendicular angle between the cross section and the fibres. The amount of fibres positioned in the specimens was selected by taking into account the volumetric fraction that entails a 6kg/m^3 addition of fibres being homogeneously distributed in the ligament of the cross section. Consequently, as the volumetric fraction that corresponds to such addition is 0.66%, the amount of fibres in a 100x100m^2 section is 66. The disposition of the fibres in the middle section of the specimens can be seen in Figure 2. No fibres were positioned in the bottom third of the specimen because such a location coincided with the position and depth of the notch. The self-compacting concrete was mixed without adding any fibre and poured in the moulds without moving or causing any damage to the long fibres positioned. The four-step process can be seen in Figure 3.

In addition to the prismatic specimens, nine cylindrical specimens were prepared with 150mm diameter and 300mm height for each batch. All the specimens were stored in a climatic chamber at 20±2ºC and above 95% of humidity until the time of testing.

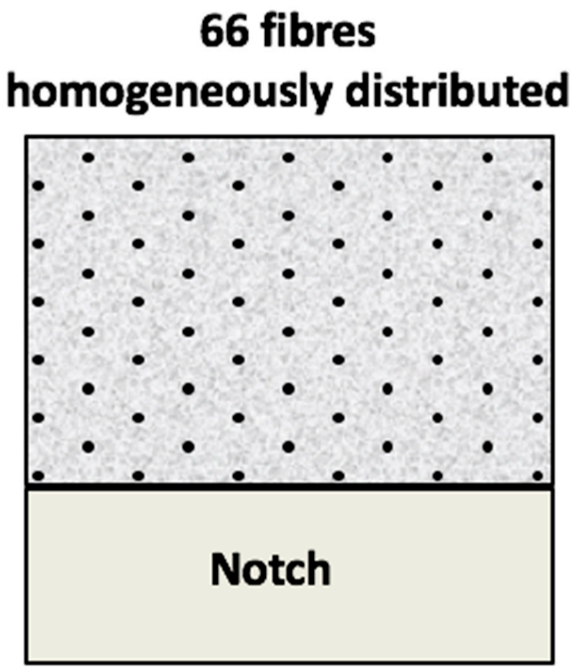

Figure 2. Cross section of the specimens performed with a homogeneous distribution of fibres.

Peer-reviewed version available at Materials 2019, 12, 220; doi:10.3390/ma12020220

Figure 3. (a) Positioning of the long fibres in the moulds; (b) fixing the mould sides to avoid any damage in the fibres while concrete in fresh state; (c) Pouring of self-compacting concrete; (d) final appearance of the specimens.

3. Material characterisation

The formulations were tested in order to obtain their main mechanical properties, such as compressive strength, indirect tensile strength and modulus of elasticity. Such tests were performed according to the following recommendations: EN 12390-3:2009 (compressive strength), EN 12390-6:2009 (indirect tensile strength) and EN 12390-13 (modulus of elasticity). Table 2 shows the mechanical properties of all the formulations performed.

Table 2. Mechanical properties of the concrete formulations.

	VCC6-60	SCC6-60	SCC6-430
Compressive strength, f_{ck} (MPa)	32.9	41.4	39.0
Modulus of elasticity, E (GPa)	29.9	31.6	36 .0
Tensile strength, f_{ct} (MPa)	3.75	4.09	3.80
Fracture energy*, G_F (N/m)	131	130	130

*Values related with its correspondent plain concrete in reference [45]

The mechanical properties shown in Table 2 show slight differences among the concrete types used. Although it can be clearly seen that the changes in the aggregate proportions and the presence of fibres caused variations in the mechanical properties, it could also be argued that such changes are of minor importance in the subject studied in this paper. That is to say, the principal effects of the orientation of the fibres appear in the post-peak region when the contribution of the concrete bulk material to the mechanical response of the composite material can be considered negligible.

The fracture tests were carried out in accordance with RILEM TC-187 SOC [46] by using three prismatic specimens for each formulation. The setup of the three-point bending test, according to the standard noted above, was made in accordance with the depth of the beam. A span-to-depth ratio of 3.0 and a notch in the centre of the span of 1/3 of the depth were chosen with the loading cylinder above the notch. The test geometry setup is shown in Figure 4.

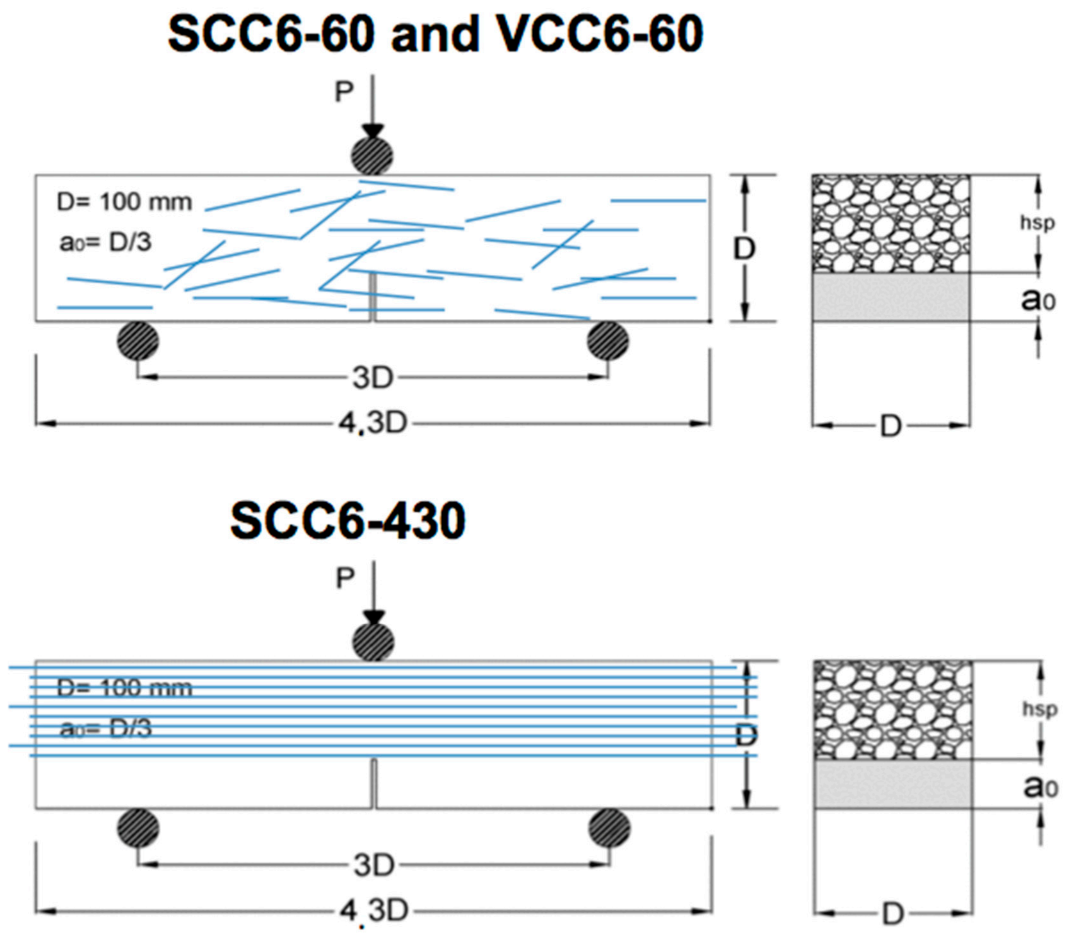

Figure 4. (a)Test geometry in the case of fibres randomly positioned; (b) test geometry in the case of fibres being aligned in the stress direction and homogeneously distributed.

The test was performed with crack-mouth opening displacement control (CMOD) by using a clip-on gauge device. Two more extensometers (linear variable differential transformer (LVDT) devices) were also placed on each side of the specimen to measure the deflection. During the test, time, load, deflection, CMOD and also the machine actuator position were recorded. Such a setup and procedure was used for testing the specimens of all formulations. An image of the testing procedure applied to a SCC6-430 specimen can be seen in Figure 5. The notch was machined with a water-cooled low-speed diamond cutting disc. The specimen positioning was carefully made by means of laser devices. The concrete beams rested on two rigid steel cylinders laying on two ground supports, which allowed free rotation out of the plane of the beam and guaranteed negligible friction rolling in the longitudinal direction of the beam. Thus, the results of the fracture tests on two beams showed a remarkably low degree of scatter. The latter is also supported by previous works in references [8, 42, 43].

Preprints (www.preprints.org) | NOT PEER-REVIEWED | Posted: 5 December 2018 doi:10.20944/preprints201812.0065.v1

Peer-reviewed version available at Materials 2019, 12, 220; doi:10.3390/ma12020220

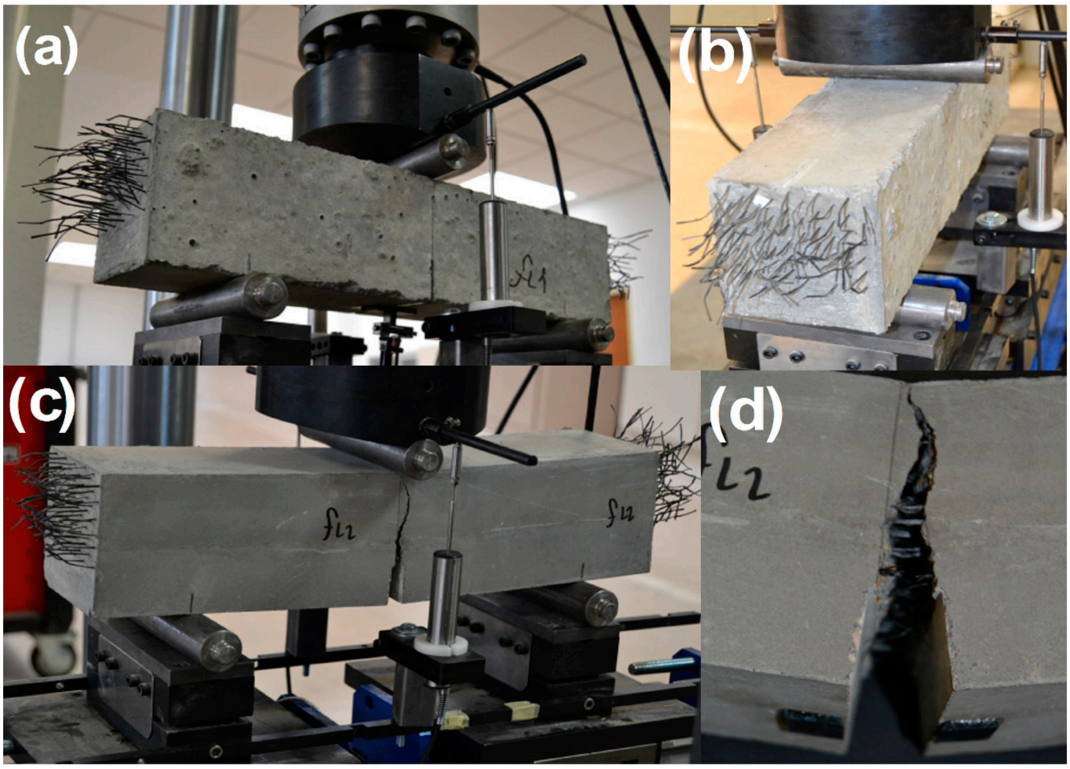

Figure 5. (a) Specimen ready for the test; (b) test disposition in the testing machine; (c) crack fully developed while testing; (d) image of the fracture surface generated in the fracture test with the fibres bridging the crack sides.

4. Fracture tests results

Regardless of the fibre rupture, fibre bridging, fibre pull-out, fibre debonding or matrix cracking, these mechanisms prompted much higher deformations in all the specimens tested than in concrete and, consequently, the upper bound of the CMOD device was exceeded. In order to continue the test, when the upper bound of the referred device was reached the control of the fracture test was changed to the machine actuator position. With the latter it was possible to obtain deflection values up to 15 mm. Nonetheless, all the tests were stopped without reaching the collapse of the specimens.

The curves obtained from the tests shown in Figure 6 could be divided in three distinct trends that can be easily identified. All can be defined by changes in the load-bearing capacity of the material. The first one begins at the start of the test and ends at the load at the limit of proportionality. Once the deflection at this point has been surpassed, an unloading branch can be perceived. The shape of such an unloading branch of the curves resembles the analogue part of the softening curve of conventional concrete. The unloading takes place until fibres are capable of absorbing the energy released in the fracture processes. The fibres added to the concrete were able to sustain higher loads and, consequently, the load-deflection curve showed a positive slope after the minimum post-peak load. Such a slope was constant from a certain deflection and afterwards, as certain damage mechanisms appeared, it decreased steadily until the maximum post-cracking load was reached. After reaching the maximum post-peak load, the load bearing capacity of the material decreases progressively due to the continuation of the damage in the material. Consequently, the load-deflection curve showed a stable reduction of the mechanical capacity of the material until the end of the test was reached.

Peer-reviewed version available at Materials 2019, 12, 220; doi:10.3390/ma12020220

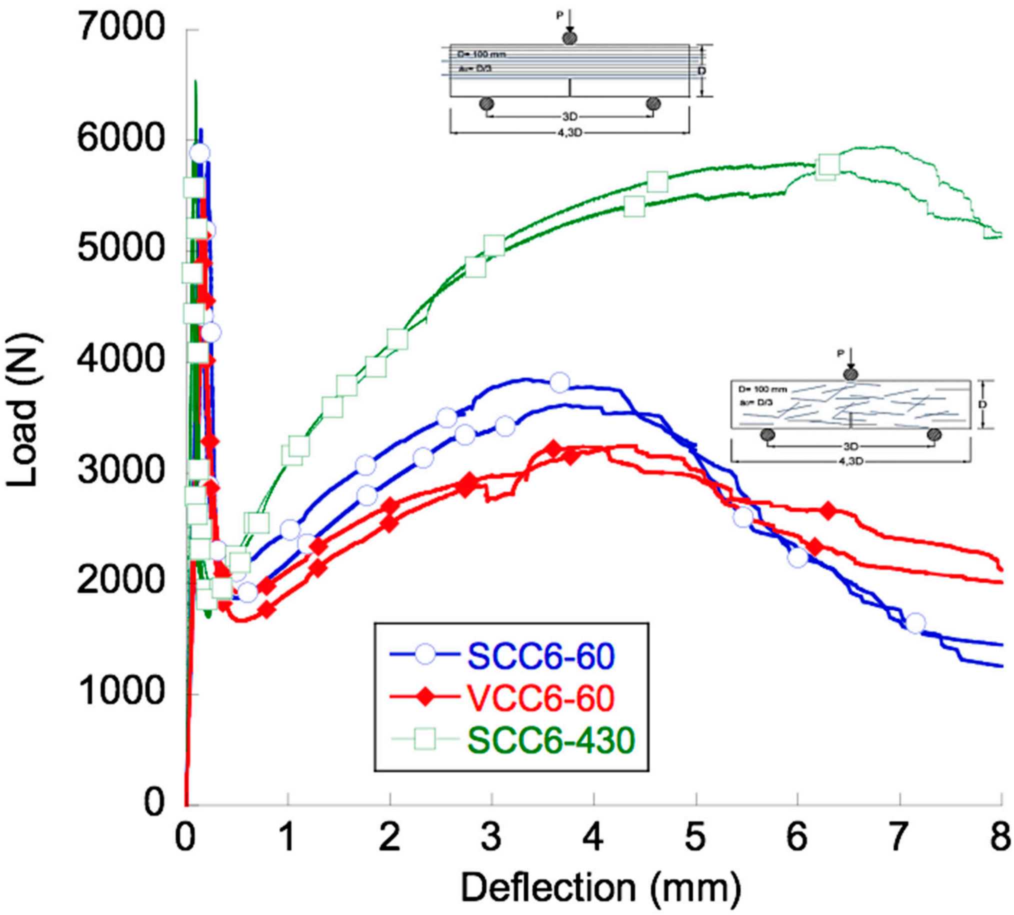

Figure 6. Three-point bending fracture test results.

The aforementioned characteristics are common for the three formulations manufactured. The mechanical response of SCC6-60 was slightly better than the VCC6-60, though no major disparities were found. In addition, such differences had already been reported in previous studies [10] and, in the case of this contribution, will be analysed by means of the orientation factor in the following sections. Nevertheless, if the fracture curves of SCC6-430 are compared with their analogous VCC6-60 and SCC6-60 remarkable features should be outlined.

There were no changes in the peak load obtained in the fracture tests. This result is coherent because there were only slight changes in the concrete formulations used. In addition, such results show that the different pouring method employed in the SCC6-60 and SCC6-430 specimens did not have any influence. Another point that should be highlighted is that in all formulations the minimum post-peak load was similar and at around 30% of the peak load.

The slope of the reloading part of the curves in the case of the SCC6-430 specimens is noticeably greater. While in the case of the VCC6-60 and SCC6-60 specimens the maximum post-peak load is around 50%, when the curves of SCC6-430 are analysed it can be seen that such s point reaches almost the value of the peak load.

In addition, the deflection at the maximum loading capacity changes from 3.5mm to 6.0mm. It has to be emphasised that this observation was already perceived to a lesser extent in previously published literature [17, 16]. When reaching this deflection, different damaging mechanisms have appeared with dissimilar importance. In the case of the concrete formulations performed with short fibres, the following damage mechanisms appear: matrix cracking, fibre-matrix debonding, fibre pull-out and fibre rupture. However, the changes of the slope that perceived when comparing the SCC6-60 and VCC6-60 curves with the SCC6-430 curves can be attributed to the damage mechanisms that cannot appear when reinforcing with long fibres: fibre pull-out. Another point worth mentioning is the lack of scattering in the case of the SCC6-430 specimens when compared with the specimens

Preprints (www.preprints.org) | NOT PEER-REVIEWED | Posted: 5 December 2018 doi:10.20944/preprints201812.0065.v1

Peer-reviewed version available at Materials 2019, 12, 220; doi:10.3390/ma12020220

performed with short fibres. This observation would clearly explain that the inherent scattering that appears in the fracture tests of FRC is caused by the differences in the amount of fibres and their positioning in the fracture surface.

Analysing the final unloading part of the tests, it can be seen that the unloading process seems to be more gradual in the case of the SCC6-430 specimens. However, a deeper study would be required to obtain sound conclusions. In any case, as in previous studies by the same authors in references [8, 10], the characteristic points of the experimental mean curves have been extracted in Table 3 in order to ease their discussion.

Table 3. Minimum (L_{MIN}) and maximum (L_{REM}) post-cracking load and their corresponding crack openings.

	L_{MIN} (kN)	w_{LMIM} (mm)	L_{REM} (kN)	w_{LREM} (mm)
SCC6-430	1.875	0.22	5.676	6.1
VCC6-60	1.788	0.54	3.246	4.1
SCC6-60	1.994	0.45	3.712	3.6

5. Fracture surface analysis

In order to quantify the importance of the orientation and distribution of the fibres, an analysis of the fracture surfaces generated in the three-point bending tests was required. In the case of the SCC6-430 specimens, the amount of fibres was predetermined in the manufacturing process to equal the theoretical one, with it having a perfect distribution and positioning. However, a fibre-counting exercise was required to assess the number of fibres in the fracture surfaces of the rest or formulations. Figure 7 shows the appearance of two specimens of VCC6-60 and SCC6-60: the notch required to perform the fracture test can be clearly seen.

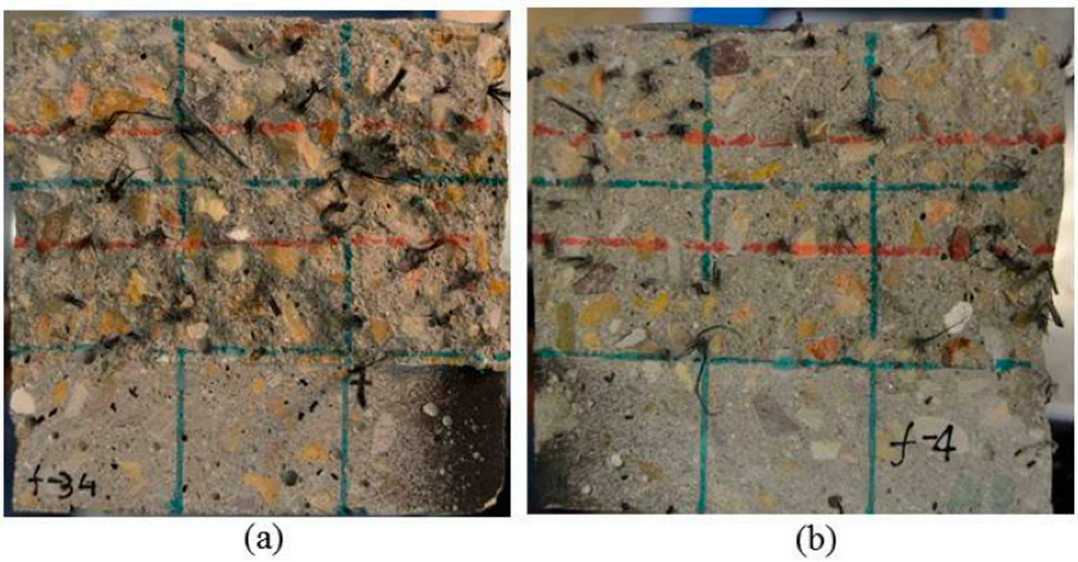

Figure 7. Fracture surfaces generated: (a) VCC6-60;(b) SCC6-60.

The theoretical number of fibres placed in the fracture surface was obtained for each concrete by using Eqs. (1) and (2), considering that the fibres were uniformly distributed and perpendicular to the crack.

$$V_f = \frac{W_f}{\rho . V} \quad (1)$$

$$th = \frac{A\, V_f}{A_f} \quad (2)$$

Preprints (www.preprints.org) | NOT PEER-REVIEWED | Posted: 5 December 2018 doi:10.20944/preprints201812.0065.v1

Peer-reviewed version available at Materials 2019, 12, 220; doi:10.3390/ma12020220

In (1) and (2) V_f is the fibre volumetric fraction, W_f the weight of the fibres for a reference volume of 1 m³, ρ the fibre density and V the total volume. In addition, th is the theoretical number of fibres placed in the fracture surface of a given specimen, with A being the cross section of the specimen and A_f the section of one fibre. The average total number of fibres obtained from the counting exercise can be seen in Figure 8. Moreover, the relation between the fibres counted in a given cross-section (n) and theoretical number of fibres (th) are also shown in Figure 8. This relation θ is the so-called in previous research orientation factor [26] that assumes a homogeneous distribution of fibres in the section and which may be seen in Eq. (3).

$$\theta = \frac{n}{th} = n\frac{A_f}{V_f A} \tag{3}$$

In the case of the SCC6-430 specimens, the theoretical fibre content was homogeneously distributed in all the specimen sections and consequently in such specimens the value of the orientation factor is 1. The evaluation of the orientation factor was performed using the approach aforementioned and the results are also shown in Figure 8, including the percentage of pull-out fibres.

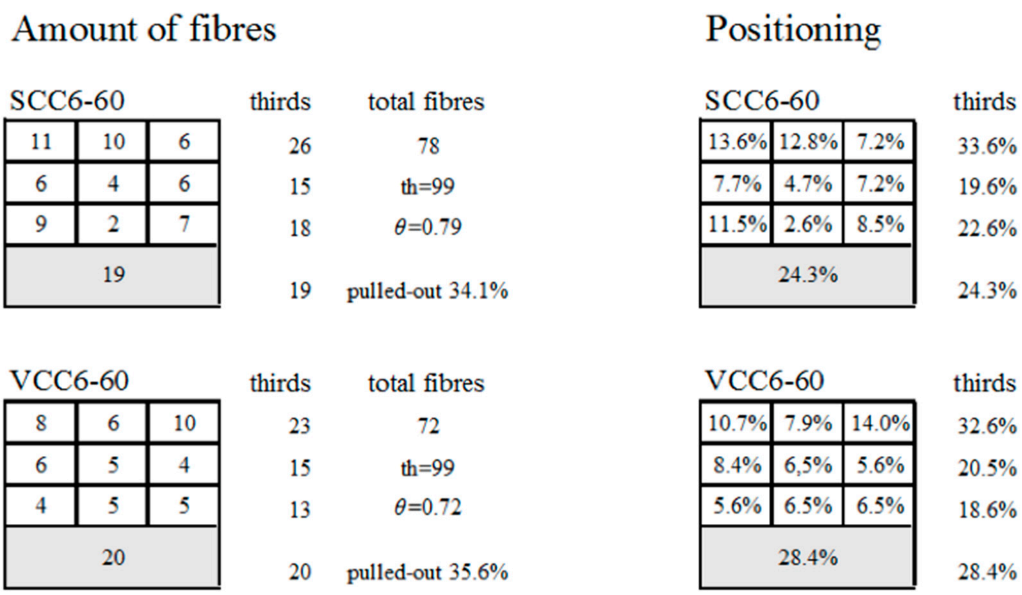

Figure 8. Counting exercise performed in SCC6-60 and VCC6-60 (including the percentage of pull-out fibres)

6. Numerical simulations

Similarly to the process followed in references [42, 43, 47], the fracture results obtained in the experimental campaign were reproduced by means of numerical simulations. This process was carried out by using the commercial software Abaqus through merging the features implemented in such a code with a material user subroutine.

The fracture behaviour was reproduced by employing 2D numerical models meshed through using three-node triangular elements with one Gauss point. The mechanical behaviour of the material implemented in the UMAT was linear elastic without any damage when under compression. Regarding the tensile behaviour, the material was linear elastic until the tensile stress was reached. If the strain that corresponds to the tensile strength were surpassed, the mechanical response of the material would be governed by a softening function implemented in a user material subroutine. As in previous studies, it was shown that a tri-linear softening function was suitable for reproducing the fracture behaviour of the material, with the same approach being used in the case of the specimens studied in this paper. The shape and the characteristic points that define the softening function can be seen in Figure 9.

Preprints (www.preprints.org) | NOT PEER-REVIEWED | Posted: 5 December 2018 doi:10.20944/preprints201812.0065.v1

Peer-reviewed version available at Materials 2019, 12, 220; doi:10.3390/ma12020220

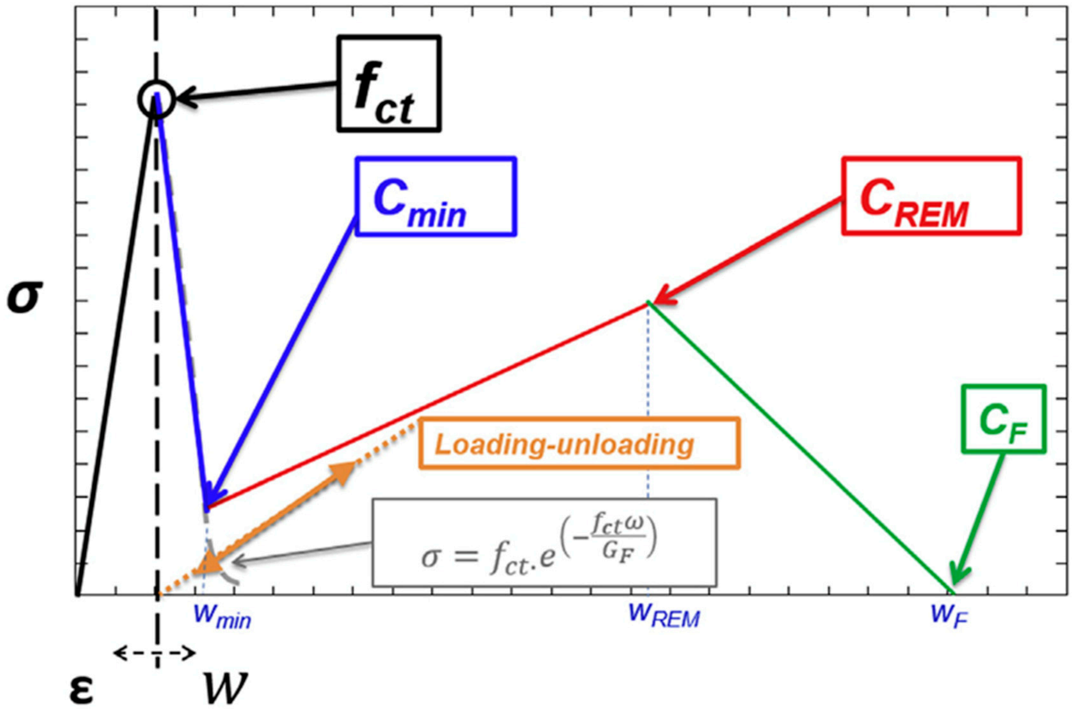

Figure 9. Sketch of the shape and position of the turning points of the constitutive relations for PFRC.

The non-linear fracture process zone emerges in the elements placed on the crack. The behaviour of the fracturing elements depends on a constitutive relation that needs to be iteratively fit until finding the values of C_{MIN}, C_{REM} and C_F that are able to reproduce the fracture behaviour of all the three formulations with a reasonable degree of accuracy.

The inverse analysis used has been explained in depth in previous papers [42]. The mechanical data of the material that was obtained in the mechanical test and used in the simulations can be seen in Table 2. For the specific fracture energy (G_F) and Poisson coefficient of plain concrete, the values of 130 N/m and 0.2 were respectively adopted [42].

With the aforementioned data and by exerting the inverse analysis previously cited, it was possible to find an accurate reproduction of the experimental tests. In addition, the tri-linear softening functions were defined. In Figure 10 both numerical results and experimental results can be seen.

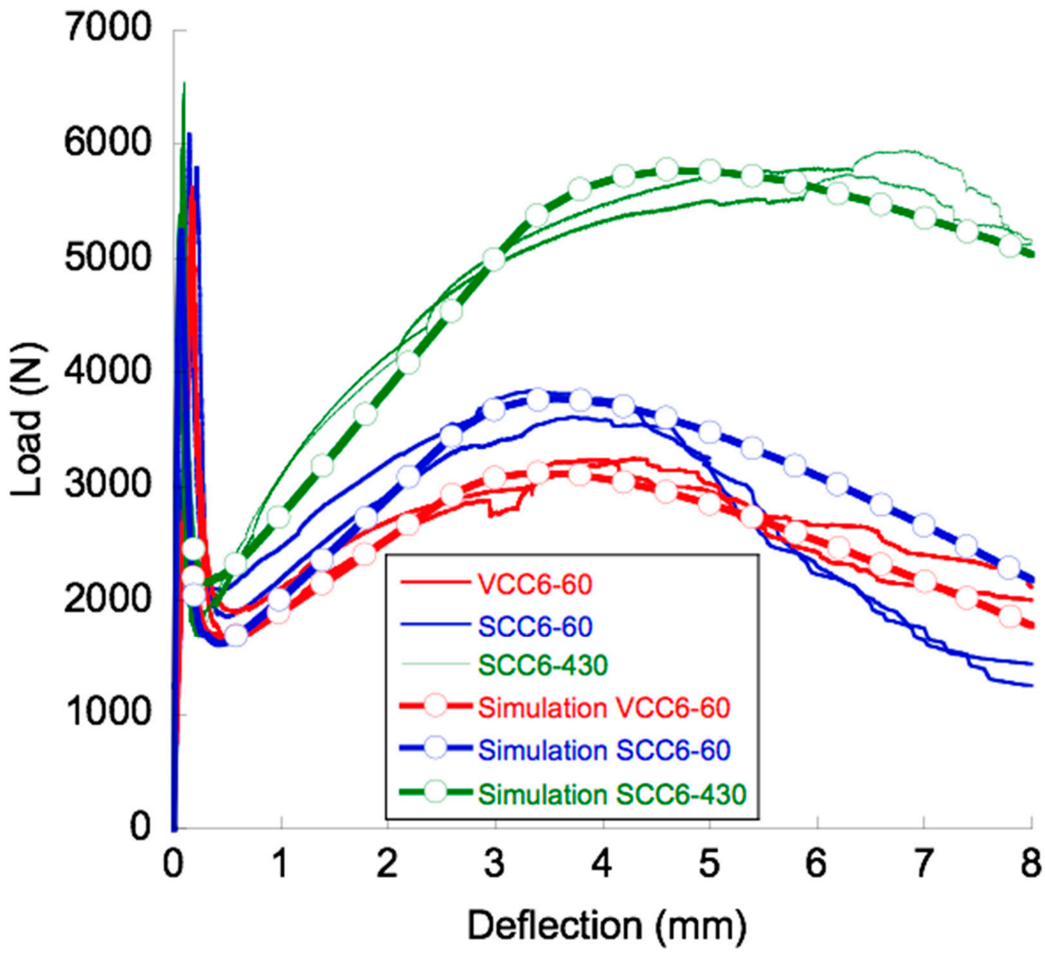

Figure 10 . Results of the numerical simulations and the experimental tests.

The curves that appear in Figure 10 clearly reproduce, and with a significant degree of accuracy, the experimental results. It should be highlighted that the accuracy of the simulations in the cases of the SCC6-60 and VCC6-60 is notable before the post-peak maximum load has been reached. However, this similarity is reduced from this point onwards. The differences that appear between the experimental curves and the numerical ones are caused by the unpredictable nature of the appearance of the aforementioned damage mechanisms. This is clearly confirmed when the scattering of the experimental curves is more reduced, as in the case of the SCC6-430 specimens. It can be clearly seen that the curves obtained by the numerical simulations in this case fits the experimental results extremely well.

The reproduction of the mechanical behaviour of SCC6-60 and VCC6-60 implied changes in f_{ct}, C_{MIN} and C_{REM}. Regarding those of C_{MIN} and C_{REM}, it can be seen in Table 4 that there were only slight changes. In the case of C_F, the value was stable for both formulations. In order to reproduce the tests of SCC6-430 specimens it was needed to change slightly the value of C_{MIN}. Nevertheless, in the case of C_{REM} not only the stress value had to be modified. The crack opening at which C_{REM} takes place changes noticeably in the specimens with the fibres homogeneously distributed and shifts from a value of 2.25 to 2.75. Similarly, the value of C_F has to be fixed at 12.5 in order to obtain an accurate reproduction of the experimental results.

Preprints (www.preprints.org) | NOT PEER-REVIEWED | Posted: 5 December 2018 doi:10.20944/preprints201812.0065.v1

Peer-reviewed version available at *Materials* **2019**, *12*, 220; doi:10.3390/ma12020220

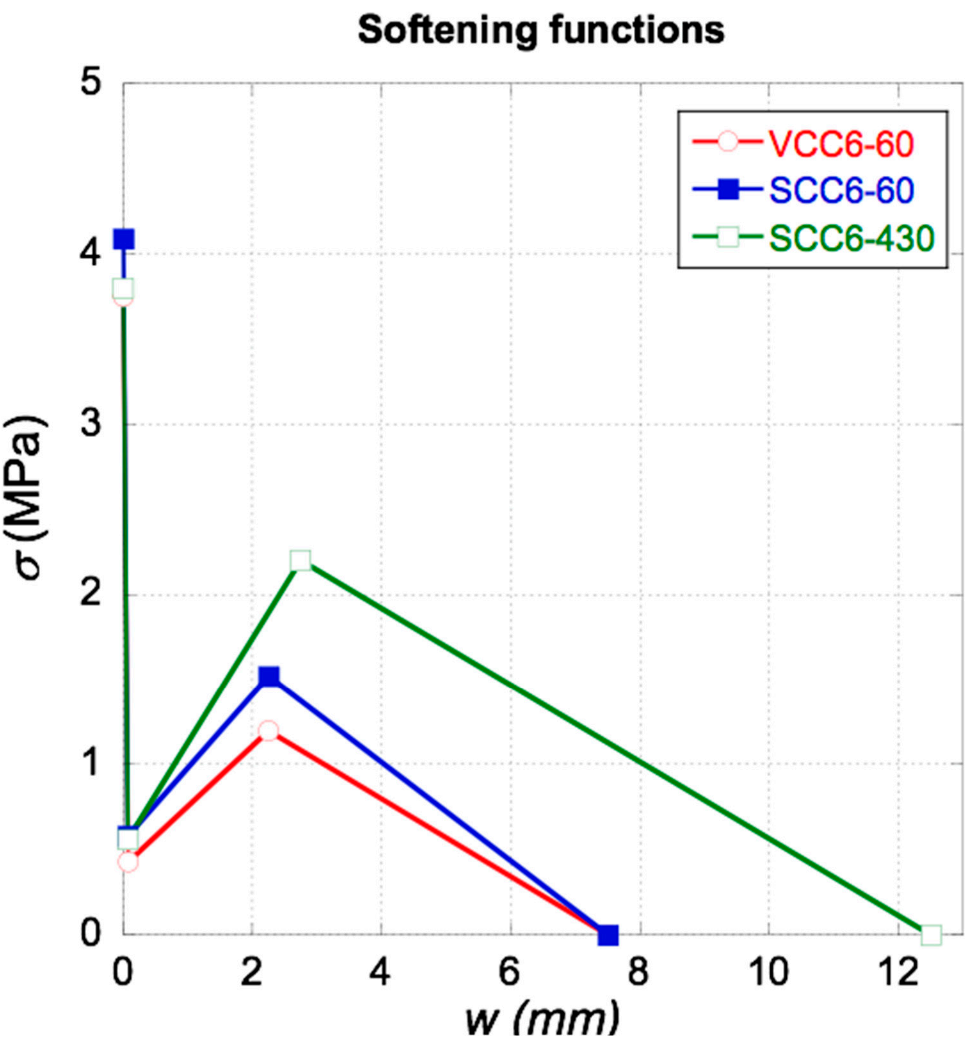

Figure 11. Softening functions implemented

Table 4. Turning points for the numerical simulation

	C_{MIN}		C_{REM}		C_F	
	w(mm)	$\sigma(MPa)$	w(mm)	$\sigma(MPa)$	w(mm)	$\sigma(MPa)$
VCC6-60	0.08	0.43	2.25	1.20	7.5	0
SCC6-60	0.07	0.58	2.25	1.52	7.5	0
SCC6-430	0.07	0.56	2.75	2.20	12.5	0

7. Discussion

This section deals with the relevant aspects of the experimental results, connections between the orientation and distribution of the fibres with such results and changes that were performed in the material subroutine implementation in order to find an accurate reproduction of all the tests.

As could be seen in the correspondent section, the general shape of the fracture curves obtained for the formulations were analogous. Both SCC6-60 and VCC6-60 were highly similar to each other. Moreover, there were significant similarities among the fracture curves of SCC6-60, VCC6-60 and SCC6-430. Although this can be seen in Figure 6, there are several aspects that should be underlined. Firstly, in all formulations the minimum post-cracking loads were similar. This feature is of primary importance because it clearly states that the bearing capacity for small deformations does not depend on the positioning or orientation of the fibres because the orientation factor of the VCC6-60 specimens on average is 0.72 and in the case of SCC6-60 is 0.78 which are noticeably smaller to the unity that the

Preprints (www.preprints.org) | NOT PEER-REVIEWED | Posted: 5 December 2018 doi:10.20944/preprints201812.0065.v1

Peer-reviewed version available at Materials 2019, 12, 220; doi:10.3390/ma12020220

SCC6-430 specimens boast. In addition, as can be seen in Figure 8 and Figure 12, although the coefficient of variation is 0.25 between the amounts of fibres in the lower third of the fracture surfaces generated, there are no remarkable changes of the value of L_{MIN} recorded. In addition, this tendency fits the previous data available in literature. Therefore, as stated in reference [42] such a load value is mainly influenced by the amount of fibres added and the rest of parameters that might be considered to have only a limited impact.

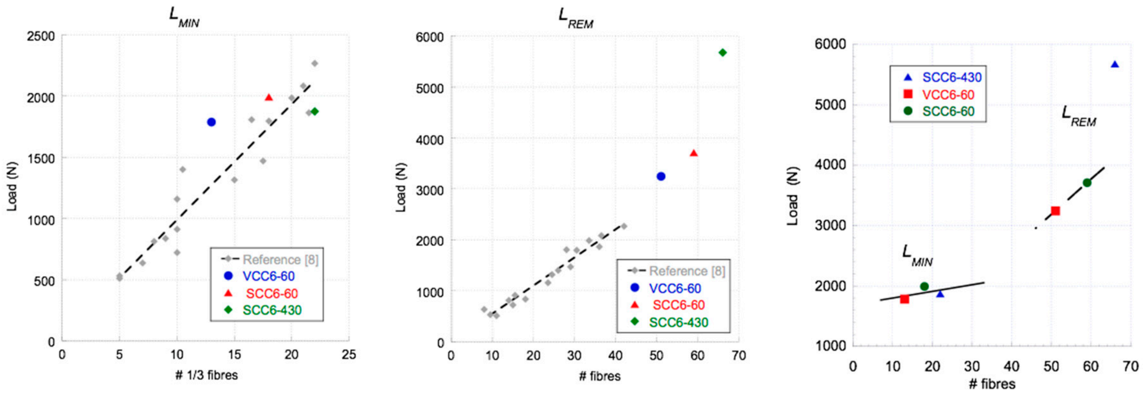

Figure 12. Relation among L_{MIN} and L_{REM} with the number of fibres in the ligament.

Another point that should be highlighted is that the slope of the reloading part of the curves is noticeably greater in the case of the SCC6-430 specimens. The slope of the SCC6-430 formulation in this part of the experimental curve is 181% higher than in the case of the VCC6-60 formulation and 156% greater than in the case of the SCC6-60. However, there was no clear relation between such increments and the difference in the presence of fibres in any of the combinations obtained by adding the amount of fibres in the thirds of the ligament surface.

Regarding the maximum post peak value, L_{REM}, it should be underlined that the experimental values obtained in the curves of the VCC6-60 and SCC6-60 specimens are above the values obtained in literature. The linear tendency that relates the amount of fibres and L_{REM} seems to be valid. Conversely, the value obtained in the case of the specimens manufactured with the 430mm-long fibres is clearly above the values or even the predictions that might be applicable to all the formulations performed with short fibres of the same characteristics. It could be argued that there were a greater number of fibres in the ligament of the specimen and thus the load that the specimens were able to sustain is also greater. Following this rationale, in the whole section there was an amount of fibres 128% and 111% greater in the case of SCC6-430 when compared with VCC6-60 and SCC6-60 respectively. However, if the values of the L_{REM} obtained for SCC6-430 is multiplied by the coefficient of orientation, the L_{REM} values of the VCC6-60 and SCC6-60 should have been 4472N and 4071N. Such values are considerably higher than those obtained. Consequently, L_{REM} values achieved by the formulations performed with 60mm-long fibres should show damage mechanisms which only appear when short fibres are added. One of such mechanisms could be the pull-out of the fibres (see reference [48]) that play a major role in the composite material behavior. Therefore, it is important to highlight that not only the orientation factor reduces the load bearing capacity of the specimen in VCC6-60 and SCC6-60 formulations.

In the case of the unloading branch of the curves, it can be seen that the unloading process is steadier in the case of the SCC6-430 specimens. While in the cases of SCC6-60 and VCC6-60 the decrement of load bearing capacity is noticeable from L_{REM} onwards, in the case of the VCC6-430 specimens it seems that this process is slower. It should be remembered that in the VCC6-430 specimens there is no possible pull-out of the fibres while this damage mechanism appears in a certain amount of fibres present in the fracture surface of SCC6-60 and VCC6-60 specimens

Regarding the numerical analysis performed, it can be concluded that only by applying minor changes in the tri-linear softening function found in the literature [42] it was possible to reproduce both the experimental results of VCC6-60 and SCC6-60 specimens. However, several changes had to be applied in order to simulate the behaviour of SCC6-430 specimens. While in the cases of the VCC6-60 and SCC6-60 specimens the changes of the values of C_{REM} were limited to the strain value, in the case of the SCC6-430 specimens it was necessary to change also the crack width where the C_{REM} takes place. Moreover, the value at which C_F takes place had to be noteworthy modified. This is in accordance with what was proposed in previous studies [11, 42, 43].

Concerning the functions derived in [11, 42], the inverse analysis performed in this contribution enabled checking of the validity of the equations deduced. If expression (1) is considered, it can be seen that the only parameter of the material is the volumetric fraction and, consequently, all the predictions of the C_{MIN} value were unique for all formulations. In Table 6 the values obtained by means of the combination of the inverse analysis and the numerical simulations are shown. As can be seen in such a table, the predicted value through using equation (1) provides an accurate fit of C_{MIN} that corresponds to VCC6-60.

$$\Phi = -3.6046 + 5.0625(1 - e^{6.55Vf}) \tag{4}$$

However, this is not the case of SCC6-60 or even SCC6-430. If the C_{MIN} value is considered as correct, the volumetric fraction could be deduced. In the case of the two formulations, such a volumetric fraction deduced corresponds to a PFRC formulation with 10 kg/m³ addition of fibres. This value could be explained if the homogeneous, and artificially prepared, disposition of the fibres were taken into account. Nevertheless, such an argument cannot be applied to the SCC6-60 result where an equal volumetric fraction of 1% is obtained. Such a remarkable variation is not only caused by the number of fibres in the lower third of the ligament, but also by the positioning of the fibres and the improvements obtained in the distribution of the fibres due to the flux of self-compacting concrete [16]. In such a lower third, the average position of the fibres was not in the centre of gravity of such an area but closer to the tip of the notch. Consequently the contribution of the fibres to regaining the load-bearing capacity was greater than in a normal situation because in average their strain was greater as it was the strain bore by them.

Considering the value of C_{REM} that can be obtained by means of expression (2), two conditions should be pointed out. While in the case of VCC6-60 and SCC6-60 the amount of pulled-out fibres and the distribution of them had to be found, with both formulations being close to 20% and 0.72 and 0.79 respectively, in the case of the SCC6-430 specimens the value of fibres pulled out is zero while the value of θ is 1. By applying these conditions to equation (2), the value of C_{REM} for all the formulations can be seen in Table 5. In the case of SCC6-60, there is an accurate prediction of the values used. However, in the case of the other two formulations there was a deviation of up to 18%.

$$\sigma_{CREM} = (1 - \%\, pulled - out\,) Vf\, \theta\, \sigma_u \tag{5}$$

Table 5. Comparison of the predicted values in references [11, 42] and those obtained in this study by inverse analysis.

	C_{MIN}			C_{REM}		
	inverse analysis	**predicted by [42]**	**Δ**	**inverse analysis**	**predicted by [42]**	**Δ**
VCC6-60	0.43	0.43	0.00%	1.20	1.42	-18.33%
SCC6-60	0.58	0.43	25.85%	1.52	1.57	-3.29%
SCC6-430	0.56	0.43	23.21%	2.20	2.48	-12.73%

Another point that should be highlighted is that with longer fibres the deflection where C_{REM} occurs changes. Such an idea was suggested when comparing the fracture test results shown in reference [16] but, due to the reduced difference in the fibre length, it was difficult to perceive. Nevertheless, when using 430mm-long fibres it has been easy to confirm this phenomenon. Even when there was a reflection in the softening function implemented. There was swift shift of 0.5mm in the case of the crack opening of the C_{REM} and in the case of C_F there was a 5mm shift. Consequently, it can be stated that the longer the fibres the greater is the value of C_F that should be implemented.

Peer-reviewed version available at *Materials* **2019**, *12*, 220; doi:10.3390/ma12020220

8. Conclusions

The failure mechanisms prompted when PFRC is subjected to a fracture test are various and complex. Such ones are fibre rupture, fibre bridging, fibre pull-out, fibre debonding or matrix cracking. Given that some of them appear at the same strain states, they compete which means that it is difficult to separate the influence of each of them. As it is hard to isolate the effect of each mechanism, the question of what would be the mechanical threshold of the reinforcement provided by the polyolefin fibres remained unsolved. This threshold is influenced by two intrinsic characteristic of the fibre reinforced concrete: the fibre distribution and the fibre orientation. In order to assess the optimum reinforcement that a certain amount of polyolefin fibres can provide, a series of tests was performed in specimens reinforced with 430mm-long polyolefin fibres perfectly distributed and oriented. The test results showed that if fibres are not pulled out, and they are homogeneously distributed, the mechanical capacity of the fibres added enables reaching stress values close to those obtained in the limit of proportionality which is also the peak load. It is also worth underlining that with such changes the performance of only 6kg/m^3 of fibres was even superior to a formulation with a 10kg/m^3 addition of short fibres.

The analysis of the fracture tests performed in the VCC6-60, SCC6-60 and SCC6-430 formulations showed that the L_{MIN} was essentially related with the amount of fibres present in the lower third of the ligament, with the uniform distribution of fibres within this third or even the length of the fibres not being of significant importance. However, when L_{REM} is considered, the behaviour of the material was greatly influenced by the fibre length due to the damage mechanisms that appear. As all the 430mm-long fibres break during the test, the amount of load that such fibres are capable of sustaining and, therefore, the amount of energy that they absorb is noticeably greater than in a standard situation. Such differences were caused by the 20% of fibres which were pulled out from the concrete matrix and the changes in the fibres positioning that appeared in VCC6-60 and SCC6-60 formulations.

Regarding the numerical simulations, the fracture tests of the formulations were reproduced and provided a remarkable degree of accuracy. The applicability of such an approach to the SCC6-430 formulation showed the robustness and versatility of the cohesive crack approach and the accuracy of the inverse analysis performed. In addition, the expressions proposed in [11, 42] have been applied to the tests conducted in this contribution with relative success. It should be noted that as the expressions had been obtained based only on a reduced amount of data the values of C_{MIN} and C_{REM} proposed were not accurate. However, if the aforementioned argument is considered, the variations of around of 25% that were assessed might be considered within the typical scattering of FRC, with them being reasonably correct and their physical meaning being considered adequate.

Lastly, the results of both the numerical simulations and experimental results have provided valuable discussion and verification of the parameters and expressions proposed in previous research as regards the influence of the coefficient of orientation. The importance of the distribution and orientation of fibres has been clearly stated, as well as the need of models and formulations that help structural designers to take into consideration this type of predictive tools and numerical results.

Acknowledgments: The authors gratefully acknowledge the financial support provided by Ministry of Economy, Industry and Competitiveness of Spain by means of the Research Fund Project BIA2016-78742-C2-2-R. They also offer their gratitude to SIKA SAU for supplying the polyolefin fibres.

References

1. R. Zollo, "Fiber-reinforced concrete: an overview after 30 years of development," *Cement & Concrete Composites*, *19*, pp. 107-122, 1996.
2. C. Lee and H. Kim, "Orientation factor and number of fibers at failure plane in ring-type steel fiber reinforced concrete," *Cement and Concrete Research*, vol. 40(5), pp. 810-819, 2010.
3. E. Nawy, Construction Engineering Handbook. 2ed., FL, USA: Taylor & Francis group., 2008.
4. D. J. Kim, A. E. Naaman and S. El-Tawil, " Comparative flexural behavior of four fiber reinforced cementitious composites," *Cement & Concrete Composites*, vol. 30(10), pp. 917-928., 2008.

5. A. Brandt, "Fibre reinforced cement-based (FRC) composites after over 40 years of development in building and civil engineering.," *Composite Structures, 86 (1-3),* pp. 3-9, 2008.
6. A. E. Naaman, "Engineered steel fibers with optimal properties for reinforcement of cement composites," *Journal of Advanced Concrete Technology,* vol. 1(3), pp. 241-252, 2003.
7. P. Garcés, E. Zornoza, L. Andión, F. Baeza and Ó. Galao, Hormigones conductores multifuncionales, Alicante, España, ISBN 978-84-9948-080-0: Editorial Club Universitario ECU, 2010.
8. M. G. Alberti, A. Enfedaque and J. C. Gálvez, "On the mechanical properties and fracture behavior of polyolefin fiber-reinforced self-compacting concrete," *Construction and Building Materials,* vol. Volume 55, pp. 274-288, 2014.
9. M. G. Alberti, A. Enfedaque, J. C. Gálvez, M. F. Cánovas and I. R. Osorio, "Polyolefin fiber-reinforced concrete enhanced with steel-hooked fibers in low proportions," *Materials & Design,* vol. 60, pp. 57-65, 2014.
10. M. G. Alberti, A. Enfedaque and J. C. Gálvez, "Comparison between polyolefin fibre reinforced vibrated conventional concrete and self-compacting concrete," *Construction & Building Materials,* vol. 85(15), pp. 182-194, 2015.
11. M. G. Alberti, "Polyolefin fibre-reinforced concrete: from material behaviour to numerical and design considerations," 2015.
12. P. Pujadas, A. Blanco, S. Cavalaro and A. Aguado, "Plastic fibres as the only reinforcement for flat suspended slabs: Experimental investigation and numerical simulation," *Construction and Building Materials,* vol. 57, pp. 92-104, 2014.
13. M. N. Soutsos, T. T. Le and A. P. Lampropoulos, "Flexural performance of fibre reinforced concrete made with steel and synthetic fibres," *Construction and Building Materials,* vol. 36, pp. 704-710, 2012.
14. K. Behfarnia and A. Behravan, "Application of high performance polypropylene fibers in concrete lining of water tunnels," *Materials & Design,* vol. 55, pp. 274-279, 2014.
15. M. G. Alberti, A. Enfedaque, J. C. Gálvez and L. Pinillos, "Structural Cast-in-Place Application of Polyolefin Fiber–Reinforced Concrete in a Water Pipeline Supporting Elements," *Journal of Pipeline Systems Engineering and Practice,* vol. 8(4), 2017.
16. M. G. Alberti, A. Enfedaque and J. C. Gálvez, "Fracture mechanics of polyolefin fibre reinforced concrete: Study of the influence of the concrete properties, casting procedures, the fibre length and specimen size," *Engineering Fracture Mechanics,* 2016.
17. M. G. Alberti, A. Enfedaque, J. C. Gálvez and V. Agrawal, "Reliability of polyolefin fibre reinforced concrete beyond laboratory sizes and construction procedures," *Composite Structures,* vol. 140(15), pp. 506-524, 2016.
18. M. G. Alberti, A. Enfedaque, J. C. Gálvez and V. Agrawal, "Fibre distribution and orientation of macro-synthetic polyolefin fibre reinforced concrete elements.," *Construction and Building Materials, ,* vol. 122, pp. 505-517, 2016.
19. P. Stroeven, "Stereology of concrete reinforced with short steel fibres," *Heron,* vol. 31(2), pp. 15-28, 1986.
20. F. Laranjeira, S. Grünewald, J. Walraven, C. Blom, C. Molins and A. Aguado, "Characterization of the orientation profile of steel fiber reinforced concrete," *Materials and structures,* vol. 44(6), pp. 1093-1111, 2011.
21. L. Martinie, P. Rossi and N. Roussel, "Rheology of fiber reinforced cementitious materials: classification and prediction," *Cement and Concrete Research,,* vol. 40(2), pp. 226-234, 2010.
22. P. Stähli, R. Custer and J. G. M. Mier, "On flow properties, fibre distribution, fibre orientation and flexural behaviour of FRC," *Materials and Structures,* vol. 41(1), p. 189–196, 2008.
23. R. Gettu, D. R. Gardner, H. Saldivar and B. E. Barragán, "Study of the distribution and orientation of fibers in SFRC specimens," *Materials and Structures,* no. 38(1), pp. 31-37, 2005.
24. B. I. G. Barr, M. K. Lee, E. J. de Place Hansen, D. Dupont, E. Erdem, S. Schaerlaekens and L. Vandewalle, "Round-robin analysis of the RILEM TC 162-TDF beam-bending test: Part 3—Fibre distribution," *Materials and Structures,* vol. 36(9), pp. 631-635, 2003.

25. M. Di Prisco, M. Colombo and D. Dozio, "Fibre-reinforced concrete in fib Model Code 2010: principles, models and test validation," *Structural Concrete,* vol. 14(4), pp. 342-361, 2013.
26. H. Krenchel, "Fibre spacing and specific fibre surface," *Fibre reinforced cement and concrete,* pp. 69-79, 1975.
27. F. Laranjeira, A. Aguado, C. Molins, S. Grünewald, J. Walraven and S. Cavalaro, "Framework to predict the orientation of fibers in FRC: a novel philosophy," *Cement and Concrete Research,* vol. 42(6), pp. 752-768, 2012.
28. fib Model Code, Model Code, Paris: Fédération Internationale du Béton fib/International Federation for Structural Concrete, 2010.
29. EHE-08, Spanish Structural Concrete Code, Spanish Minister of Public Works, 2008.
30. RILEM- TC 162-TDF, "Test and design methods for steel fibre reinforced concrete," *Materials and Structures,* vol. 33, pp. 75-81, 2000 .
31. CNR-DT 204, "Guide for the design and construction of fiber-reinforced concrete structures," Consiglio Nazionale delle Riserche, Roma, 2006.
32. ASTM C 1609/C 1690M-07, "Standard test method for flexural performance of fiber reinforced concrete (using beam with third-point loading)," p. 1–8, 2007.
33. EN 14651:2005+A1:2007, Test method for metallic fibre concrete. Measuring the flexural tensile strength (limit of proportionality (LOP), residual), 2007.
34. EN 14889-2, Fibres for concrete.Polymer fibres. Definitions, specifications and conformity, 2008.
35. M. C. Torrijos, B. E. Barragán and R. L. Zerbino, "Placing conditions, mesostructural characteristics and post-cracking response of fibre reinforced self-compacting concretes," *Construction and Building Materials, 24(6),* p. 1078–1085, 2010.
36. R. Zerbino, J. M. Tobes, M. E. Bossio and G. Giaccio, "On the orientation of fibres in structural members fabricated with self compacting fibre reinforced concrete.," *Cement and Concrete Composites, 34(2),* p. 191–200, 2012.
37. M. G. Alberti, A. Enfedaque and J. C. Gálvez, "On the prediction of the orientation factor and fibre distribution of steel and macro-synthetic fibres for fibre-reinforced concrete," *Cement and Concrete Composites,* 2016.
38. D. Dupont and L. Vandewalle, "Distribution of steel fibres in rectangular sections," *Cement and Concrete Composites,* vol. 27(3), pp. 391-398, 2005.
39. P. Soroushian and C. D. Lee, "Distribution and orientation of fibers in steel fiber reinforced concrete," *ACI Materials Journal,* vol. 87(5), 1990.
40. J. A. Barros, V. M. Cunha, A. F. Ribeiro and J. A. B. Antunes, "Post-cracking behaviour of steel fibre reinforced concrete," *Materials and Structures,* vol. 38(1), pp. 47-56, 2005.
41. D. Y. Yoo, S. T. Kang and Y. S. Yoon, "Effect of fiber length and placement method on flexural behavior, tension-softening curve, and fiber distribution characteristics of UHPFRC," *Construction and Building Materials,* vol. 64, pp. 67-81, 2014.
42. M. G. Alberti, A. Enfedaque, J. C. Gálvez and E. Reyes, "Numerical modelling of the fracture of polyolefin fibre reinforced concrete by using a cohesive fracture approach," *Composites Part B: Engineering,* 2016.
43. A. Enfedaque, M. Alberti, J. Gálvez and M. Beltrán, " Constitutive relationship of polyolefin fibre–reinforced concrete: Experimental and numerical approaches to tensile and flexural behaviour," *Fatigue & Fracture of Engineering Materials & Structures,* 2017.
44. EN 197-1 , Cement – Part 1: Composition, specifications and conformity criteria for common cements, European Committee for Standardization, 2011.
45. M. Alberti, V. E. A. Agrawal and J. Gálvez, "Hormigón reforzado con alto contenido de fibras de poliolefina," in *Anales de Mecánica de la Fractura*, 2014.
46. RILEM TC-187-SOC, "Indirect test for stress-crack opening curve," 2007.
47. A. Enfedaque, M. Alberti, J. Gálvez and J. Domingo, "Numerical simulation of the fracture behaviour of glass fibre reinforced cement," *Construction and Building Materials,* vol. 136, pp. 108-117, 2017.

 doi:10.20944/preprints201812.0065.v1

Peer-reviewed version available at *Materials* **2019**, *12*, 220; doi:10.3390/ma12020220

48. M. G. Alberti, A. Enfedaque, J. C. Gálvez and A. Ferreras, "Pull-out behaviour and interface critical parameters of polyolefin fibres embedded in mortar and self-compacting concrete matrixes," *Construction & Building Materials*, 2016.